# Sentinel-1A: Flight Dynamics Analysis of the August 2016 Collision Event

By Petr KUCHYNKA,[1,a)] Miguel Angel MARTIN SERRANO,[1,b)] Mikel CATANIA,[1,c)] Xavier MARC,[1,d)] Dirk KUIJPER,[1,e)] Vitali BRAUN,[2,a)] and Holger KRAG[2,b)]

[1)] *Flight Dynamics Division, European Space Operations Center, ESA (GMV INSYEN [a)], SCISYS [b)], LSE [c)], ESA [d)], CGI [e)]), Darmstadt, Germany*

[2)] *Space Debris Office, European Space Operations Center, ESA (ESA [a)], IMS [b)]), Darmstadt, Germany*

Sentinel-1A is a low Earth orbit satellite launched on the 3rd of April 2014 and operated by the European Space Operations Center in the framework of the Copernicus earth observation program. On the 23rd of August 2016, the satellite experienced a collision with a small space particle. The event appeared in the telemetry data and was confirmed by a picture of the solar wing taken with an on-board camera. This paper summarizes the analysis of the collision event from the perspective of the Flight Dynamics team. We describe the set of data and methodology used to estimate the linear momentum of the impacting particle and the corresponding uncertainty. We also constrain the particle size from the momentum uncertainty distribution and simple considerations on the particle trajectory.

**Key Words:** Sentinel, Collision, Flight Dynamics, Space Debris

## 1. Introduction

Sentinel-1A and 1B form a 2-satellite, all-weather, day-and-night, radar monitoring system operated from the European Space Operations Centre (ESOC) in Darmstadt, Germany. The spacecraft belong to the fleet of satellites operated in the framework of the European Commission's earth observation program Copernicus, previously named GMES. The Sentinel-1 mission is described in Ref. 1). Each spacecraft provides land and ocean observations through a synthetic aperture radar (SAR) instrument. This monitoring system replaces radar data provided by the now terminated ERS and Envisat missions.

The spacecraft follow the same dawn-dusk Sun-synchronous reference orbit at about 700 km altitude with a phase difference of 180 deg. The strict mission orbit control requirements are achieved by the execution of weekly maneuvers. The maneuver implementation process is highly automated. In the flight dynamics (FD) system, it involves a manual intervention the day of the command generation and a manual performance check on the day following the maneuver execution. During one of these routine checks, on the 25th of August 2016, the FD team noticed a degradation for Sentinel-1A in the quality of the GPS-based orbit determination. The cause was tracked down to an unexpected event in GPS data occurring on the 23rd of August at 17:07 UTC and equivalent to a velocity change of 0.7 mm/s against the flight direction. Further investigation revealed a series of simultaneous features in the housekeeping telemetry of the attitude and orbit control system (AOCS): spikes in attitude rates, unexpected reaction wheels actuation and star tracker freezes. In parallel, on the 25th of August, the Sentinel-1A Flight Control Team announced a drop in the output current of the forward solar array wing. A few days later, a picture taken by one of the on-board cameras revealed damage to the solar wing and confirmed the hypothesis of a collision with a space particle. A thorough investigation of the event concluded that the damage incurred by the spacecraft had little effect on its overall health and did not affect the capacity to accomplish its mission.

This paper provides a FD analysis of the collision event. The objective is twofold. First, to present the AOCS telemetry readings of the event and deduce the magnitude and direction of the linear momentum of the impacting particle. Second, to show that the obtained result, combined with simple considerations on the particle trajectory, leads to relatively tight constraints on the particle size.

## 2. Spacecraft

### 2.1. Orbit

The orbit control strategy is described in Ref. 2). Orbit control requirements are achieved by following a reference orbit with a repeat cycle of 12 days and 175 orbits per cycle (see Tab. 1). This allows a revisit time of the 2-satellite constellation of 3 days at the equator and less than 2 days at Europe's latitudes. Mission orbit control requirements are achieved by controlling the ground-track and the eccentricity of the spacecraft through weekly maneuvers in order to maintain its trajectory within a tube of 130 m of radius. This has been relaxed from an initial radius of 50 m. Ground track at the equator and at maximum latitude is maintained within 120 m of the reference. Eccentricity difference at the ascending node is kept under $10^{-5}$.

Table 1. Characteristics of the Sentinel-1A reference orbit.

| | |
|---|---|
| Period | 98.742 min |
| Eccentricity | frozen eccentricity vector |
| Inclination | near polar/Sun-synchronous |
| Local time at asc. node | 18:00 (dusk-dawn) |

### 2.2. Attitude

The frames relevant for the analysis and the spacecraft attitude during the collision are illustrated on Fig. 1. The figure also indicates the position of the impact on the forward solar array wing.

The spacecraft reference (REF) and body frames are defined by axes attached to the spacecraft. The x-axis is aligned with the rotation axis of the solar arrays. The z-axis points from the

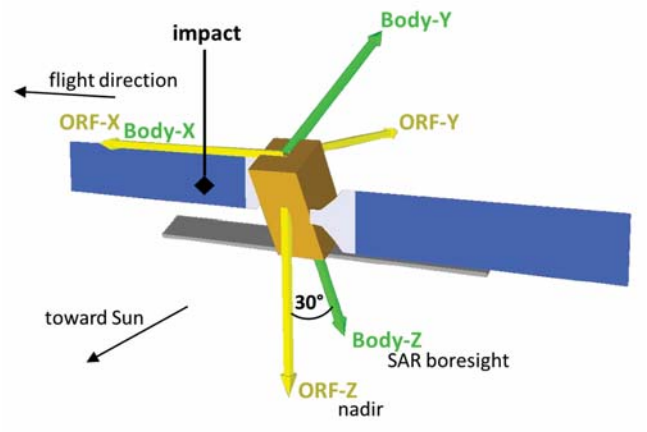


Fig. 1. Sentinel-1A at the time of the impact. For clarity, the origins of the ORF and body frames are not represented at the center of mass, but at the origin of the REF frame.

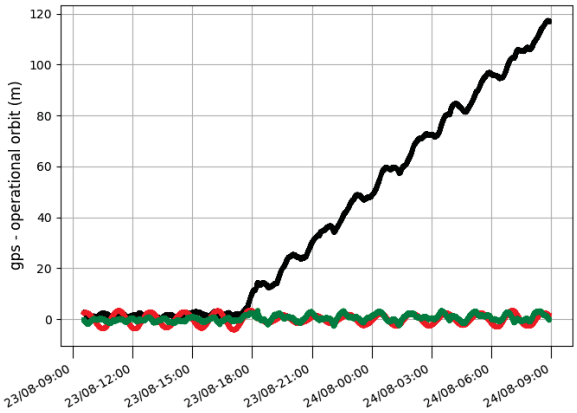


Fig. 2. Difference in position between GPS data and the on-ground operational orbit. The components, x/along track (black), y/cross track (red) and z/radial (green), are expressed in the ORF frame of the operational orbit.

spacecraft interface ring towards the SAR and the y-axis completes the frame. The REF and body frames are centered respectively at the interface ring and the spacecraft center of mass, otherwise they are identical. The orbital reference frame (ORF) is centered at the spacecraft center of mass, its x-axis points along the inertial velocity while the y-axis is parallel and opposite to the orbit normal. The z-axis completes the frame and points towards the Earth. The solar arrays are rotated by +30 deg around the x-axis of the body frame in order to compensate for the off-nadir pointing of the instrument. Note that the solar arrays were rotated after launch and since they remained in a fixed position.

At the time of the collision event, the spacecraft was in normal pointing mode (NPM). The attitude of the body frame is then roughly given by a rotation of the ORF frame around the x-axis. The exact body frame attitude is defined by a rotation of -29.45 deg around the x-axis of the so-called Zero-Doppler frame. The frame differs from ORF by up to 4 deg. In NPM, the spacecraft also follows a roll-steering law with a maximum amplitude of 0.6 deg. The roll steering guarantees a constant slant range of the radar beam throughout the orbit, despite variations of the spacecraft altitude with respect to Earth's ellipsoid. The collision occurs near the south pole at an argument of latitude of 288 deg, where the misalignment of the Zero-Doppler frame and the orbital frame is close to 1 deg. In the following analysis, the misalignment and the roll steering effects are neglected. We consider that the spacecraft body frame coincides with the ORF frame rotated by -30 deg around the x-axis. This assumption will be justified later by the large uncertainty in the linear momentum of the impacting particle.

### 2.3. Mass properties

The spacecraft mass at the time of the collision event is given by its total dry mass, initial fueling conditions and the estimate of fuel consumption since launch. The total mass amounts to:

$$M = 2147.343 \quad \text{(kg)}. \tag{1}$$

The estimation of fuel mass distribution leads to a center of mass position (in REF),

$$\vec{G} = \begin{pmatrix} 0.004 \\ -0.009 \\ 2.010 \end{pmatrix} \quad \text{(m)}, \tag{2}$$

and an inertia matrix (in body frame),

$$I = \begin{pmatrix} 3500 & -414 & 64 \\ -414 & 16688 & -29 \\ 64 & -29 & 13811 \end{pmatrix} \quad \text{(kg m}^2\text{)}. \tag{3}$$

The inertia matrix is computed with respect to the body frame origin.

## 3. Data

### 3.1. AOCS telemetry

The collision is recorded in the evolution of several AOCS housekeeping parameters monitored by the FD team.

A parameter that is routinely monitored is the difference between GPS data and the operational orbit, that is the difference between the spacecraft measured position and its predicted trajectory. The evolution for the 23rd of August 2016 is reproduced in Fig. 2. Throughout the paper, we use the convention of providing time in UTC. This also applies to all figures. At approximately 17:00, a linear drift is introduced in the along-track direction. The drift may be interpreted as a sudden change in the semi-major axis or, equivalently, a change in velocity. The drift reaches 120 m in about 16 hours. This corresponds to 12.4 m per orbital period or, equivalently, a shortening of the orbital period by 0.0016 s. The differentiation of Kepler's law gives

$$\Delta a = \frac{2a}{3T}\Delta T, \tag{4}$$

where $a$ and $T$ represent the semi-major axis and the corresponding period. With the values in Tab. 1, we obtain $\Delta a$=1.3 m equivalent to $\Delta V$=0.7 mm/s. The direction of the drift indicates that the spacecraft is moving faster than the operational orbit. The introduced change in semi-major axis is negative. The corresponding $\Delta V$ is thus against the flight direction.

In order to derive an associated uncertainty, the velocity change is estimated by running an orbit determination process with an artificial instantaneous maneuver introduced at 17:00. If the maneuver's components are left as free parameters, the orbit determination provides formal uncertainties on the components. In order to derive realistic uncertainties, the orbit determination is run first with a fixed maneuver size of 0.7 mm/s. This leads to clean residuals with the typical magnitude of 2 m expected from

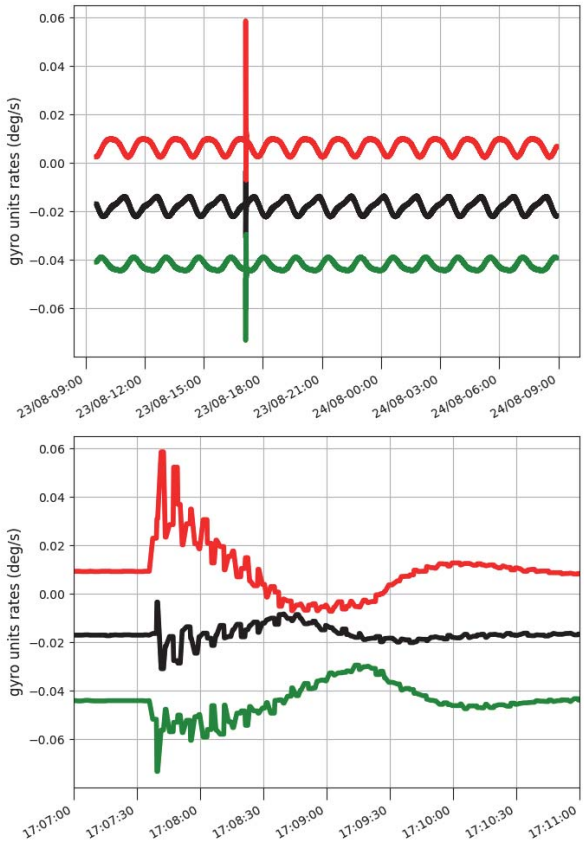


Fig. 3. Rate measurements of the active gyro units: unit #1 (black), unit #2 (red) and unit #3 (green).

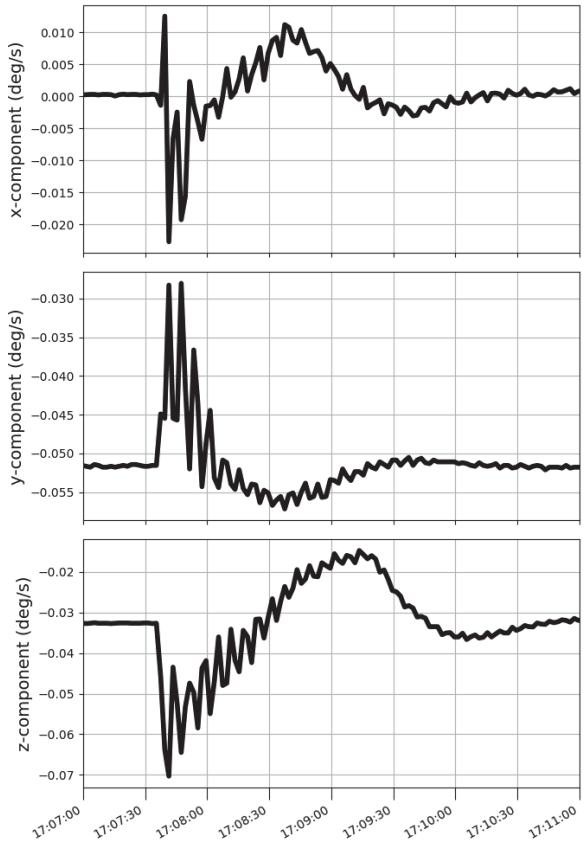


Fig. 4. Components of the angular velocity vector in the body frame derived from the gyro units readings.

GPS data in the routine orbit determination. Each component of the maneuver is then progressively increased until a visible degradation of the residuals is observed. The process leads to the following estimate of the equivalent velocity change and the associated uncertainty (in ORF):

$$\Delta\vec{V} = \begin{pmatrix} -0.7 \\ 0 \\ 0 \end{pmatrix} \pm \begin{pmatrix} 0.1 \\ 10 \\ 2 \end{pmatrix} \quad \text{(mm/s)}. \tag{5}$$

A drift of GPS values with respect to the operational orbit is not necessarily caused by an actual change in the spacecraft velocity. The operational orbit is composed of arcs spanning 1 day from 18:00, each resulting from an orbit determination based on the latest available data. The orbit is propagated for several days beyond the last available data point. Thus the observed drift could result from an imperfect parameter estimation or from an imperfect parameter used in the propagation.

In general, the telemetry data presented in this section is given as it appeared to the FD team during the investigation of the collision event. Fig. 2 depends on the actual telemetry, but also on the operational orbit. Contrary to telemetry data, the history of the operational orbit is not archived. The orbit is updated daily and its exact state at the time of the investigation is in practice lost. The evolution in the presented figure has been obtained by re-running the orbit determination process on GPS data spanning until 17:00 of August 23$^{\text{rd}}$. This was approximately the case when the collision was investigated. A screenshot of the plot as it originally appeared to the FD team is available in Ref. 3).

Similarly to the spacecraft position, the attitude is monitored by comparing attitude measurements from star-trackers to the ideal attitude expected in NPM. The evolution of the comparison is not shown because the only features would be gaps of 10 min and 20 min in the readings of the 2 active star-trackers. The start of both gap intervals coincides with an abrupt change in attitude rates recorder by the gyro units and shown on Fig. 3. The evolution of the gyro rates translated into components of the angular velocity vector in the body frame is plotted in Fig. 4. The sudden change of angular velocity is absorbed within the next 3 min by the actuation of reaction wheels, see Fig. 5. Both the actuation of the reaction wheels and the attitude rates exhibit simultaneously an abrupt change. However, the change in the angular velocity is almost instantaneous indicating the spacecraft is subject to a large torque during a very short duration. In contrast, the actuation of the reaction wheels consists in a constant acceleration over a duration of almost 1 min. Thus the actuation is a consequence of the change in attitude and not its cause. The change in angular velocity is accompanied by a damped oscillation of about 0.1 Hz. Given the damped nature of the oscillation, the effect may be generated by the vibration of the solar arrays. The observed frequency is also of the expected order of magnitude, see Ref. 4). A visual inspection of Fig. 4 leads to the following estimate of the change in angular velocity and its associated uncertainty (in body frame),

$$\Delta\vec{\Omega} = \begin{pmatrix} -0.005 \\ 0.015 \\ -0.025 \end{pmatrix} \pm \begin{pmatrix} 0.01 \\ 0.01 \\ 0.01 \end{pmatrix} \quad \text{(deg/s)}. \tag{6}$$

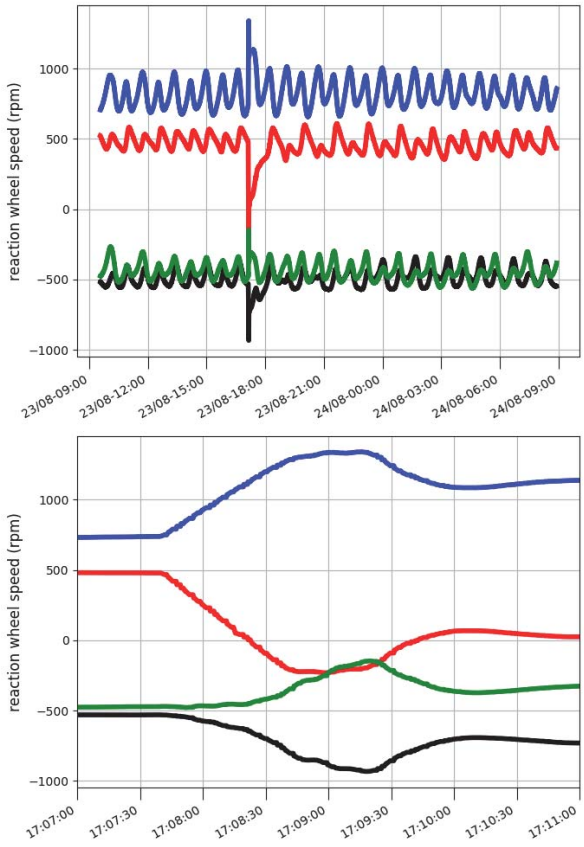


Fig. 5. Rotation speeds of the reaction wheels: wheel #1 (black), wheel #2 (red), wheel #3 (green) and wheel #4 (blue).

The simultaneous occurrence of a sudden change in velocity and attitude, measured by independent sensors (GPS and gyro units) confirms a real event experienced by the spacecraft. The term real is understood here in contrast to an artifact related to ground or on-board software. The star-tracker validity flags provide an exact timing of the event. Both star-trackers become invalid at 17:07:37. This is the earliest imprint of the collision event on the telemetry.

### 3.2. Additional data

The correlation of changes in the telemetry occurring at the same time does by itself not provide enough information to conclude the spacecraft was hit by a space particle. An uncommanded actuation or sudden out-gassing would have a similar effect. The confirmation of the collision was provided by the flight control team announcing a sudden drop in power in the forward solar array wing. This prompted the activation of an on-board camera, initially installed to confirm the correct deployment of the panels after separation. This picture is shown on Fig. 6. A face-on view projection computed in Ref. 3) is reproduced in Fig. 7. Based on the dimensions of the spacecraft in the manufacturer documentation, the visual inspection of the camera picture and Eq. 2, we estimate the position of the damaged part of the solar panel. The corresponding components are (in body frame):

$$\vec{r} = \begin{pmatrix} 4.64 \\ 0.45 \\ -0.26 \end{pmatrix} \pm \begin{pmatrix} 0.25 \\ 0.25 \\ 0.25 \end{pmatrix} \quad \text{(m)}. \tag{7}$$

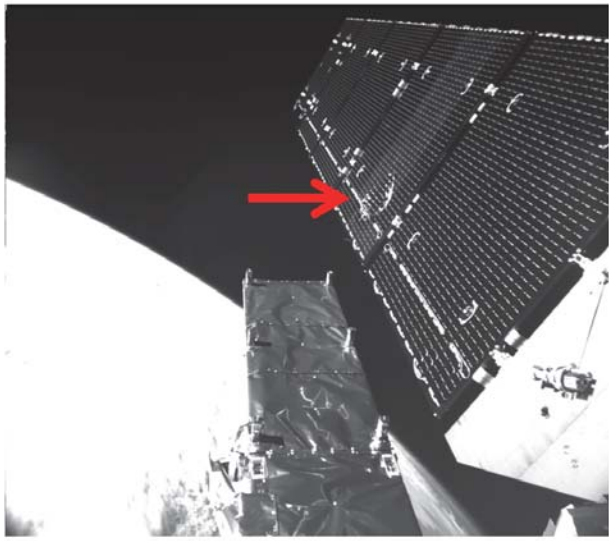

Fig. 6. Picture of the damaged forward solar array wing taken by the on-board camera. The arrow indicates the damaged area.

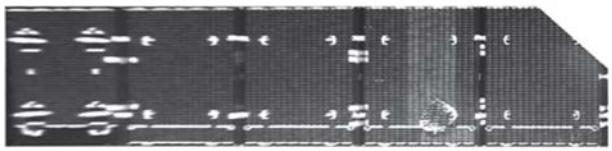

Fig. 7. Face-on view of the damaged solar array wing obtained by re-projecting Fig. 6. The damage is visible on the second panel from the right.

## 4. Collision analysis

### 4.1. Linear momentum of the impacting particle

The objective of this section is to use the available data to determine the linear momentum of the impacting particle. Two hypotheses are introduced:

- During a short interval around collision time, the body frame of a virtual spacecraft subject to no collision may be considered as an inertial frame.
- The collision is perfectly inelastic: all the momentum of the particle is transferred to the spacecraft.

The body frame of the virtual spacecraft will be used for applying the conservation of linear and angular momentum. Before the collision, this frame coincides with the body frame of the actual spacecraft. The first hypothesis is not perfectly valid. However, over a short interval around collision time, the variations of the linear and angular momentum introduced by the non-inertial character of the frame considered as inertial will introduce negligible errors in the conservation laws. The second hypothesis is more problematic: it is not guaranteed that the particle did indeed remain lodged in the solar panel and did not go through carrying away some significant momentum. As discussed in Ref. 3), several fragments have been released by the impact and are currently tracked by the U.S. Strategic Command. In the following, we assume that the momentum carried away by these fragment is negligible.

#### 4.1.1. Methodology

Let's write in the inertial frame the conservation of linear and angular momentum, for the system constituted by the spacecraft

and the impacting particle:

$$\vec{p} = m\vec{v} = M\Delta\vec{V}, \tag{8}$$

where $\vec{p}$ is the momentum of the particle, $m$ its mass and $\vec{v}$ its velocity, $M$ is the mass of the spacecraft and $\Delta\vec{V}$ the velocity change resulting from the collision. Similarly we have:

$$\vec{L} = \vec{r} \times \vec{p} = I\Delta\vec{\Omega}. \tag{9}$$

Where $\vec{L}$ is the angular momentum of the particle, $\vec{r}$ the position of the impact, $I$ the inertia matrix of the spacecraft and $\Delta\vec{\Omega}$ the change in angular velocity. The expression $I\Delta\vec{\Omega}$ for the angular momentum is valid in the body frame whose attitude changes because of the impact. As mentioned earlier, the rotation is so slow that considering $I\Delta\vec{\Omega}$ expressed in the inertial frame introduces negligible errors.

We use the $_x$, $_y$ and $_z$ indices to denote vector components. With $M$ and $\Delta V_x$ known, the equation in linear momentum allows estimating $p_x$:

$$p_x = M\,\Delta V_x. \tag{10}$$

If $\vec{r}$, $I$ and $\Delta\vec{\Omega}$ are known, the equation in angular momentum allows estimating the remaining components:

$$\begin{aligned} p_y &= \frac{(I\Delta\vec{\Omega})_z - r_y p_x}{r_x} \\ p_z &= \frac{(I\Delta\vec{\Omega})_y - r_z p_x}{-r_x}. \end{aligned} \tag{11}$$

This first estimate of $\vec{p}$ may be improved and, more importantly, complemented with uncertainties by expressing the measurements of $\Delta\vec{V}$, $\Delta\vec{\Omega}$ and $\vec{r}$ as functions of $\vec{p}$ and $\vec{r}$. The uncertainty in the spacecraft mass properties is negligible. Linearizing around reasonable values of $\vec{p}$ and $\vec{r}$ allows deriving the uncertainties on the parameters through the least-squares framework.

Let's denote with $\gamma$ the measurement vector defined as:

$$\gamma = \begin{pmatrix} \Delta\vec{V} \\ \Delta\vec{\Omega} \\ \vec{r} \end{pmatrix}. \tag{12}$$

The dependency of $\gamma$ on $\vec{p}$ and $\vec{r}$ is given by Eq. 8 and Eq. 9. Note that $\vec{r}$ is at the same time a parameter and a measurement. This corresponds to introducing a priori uncertainties in the fit, or, equivalently using regularization. The approach is fairly classical. Its use in the present paper is similar to previous work in Ref. 5) where the theoretical framework is described in more detail.

Let's define $\beta$ as the parameter vector:

$$\beta = \begin{pmatrix} \vec{p} \\ \vec{r} \end{pmatrix} \tag{13}$$

Linearizing $\gamma$ around some reasonable value of $\beta_0$ leads to

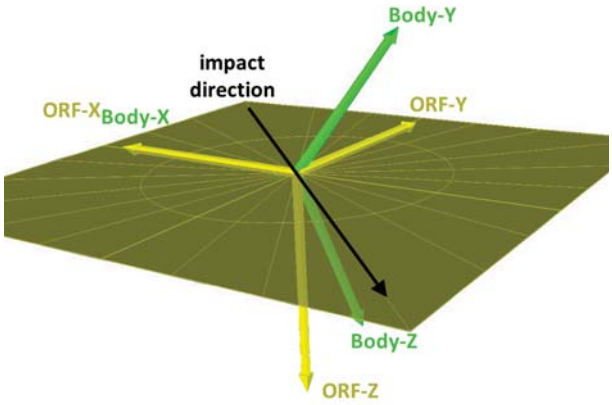


Fig. 8. Estimated impact direction in a frame with origin at the spacecraft center of mass.

$$\begin{aligned} \beta &= \beta_0 + \delta\beta, \\ \gamma &= \gamma_0 + A\,\delta\beta, \end{aligned} \tag{14}$$

where $A$ is a partials matrix and $\gamma_0$ the value of the measurement vector for $\beta_0$. The least squares framework allows adjusting $\delta\beta$ in order to reduce the difference between the predicted measurements $\gamma$ and the actual measurements $\gamma_m$:

$$\delta\beta = (A^T A)^{-1} A^T (\gamma_m - \gamma_0). \tag{15}$$

The covariance of $\delta\beta$ is then given by

$$\mathrm{Cov}(\delta\beta) = (A^T A)^{-1}. \tag{16}$$

The uncertainties of the parameters are the square roots of the diagonal elements of $\mathrm{Cov}(\beta)$. In order for the least squares to be efficient (best linear unbiased estimator), the measurement vector and the corresponding partial matrix need to be weighted by their respective uncertainties. More specifically, $\gamma$ and $\gamma_0$ need to be replaced by $W\gamma$ and $W\gamma_0$, where $W$ is a matrix such that $\mathrm{Cov}(W\gamma_m)$ is the identity. Similarly, $A$ needs to be replaced by $WA$. For uncorrelated measurements, $W$ is diagonal with each diagonal element equal to the inverse of the measurement 1-sigma uncertainty.

#### 4.1.2. Results

A first estimate of $\beta$ is obtained from Eq. 10 and Eq. 11 as well as the values of $\Delta\vec{V}$, $\Delta\vec{\Omega}$ and $\vec{r}$ in Eq. 5, Eq. 6 and Eq. 7. Using the first estimate as $\beta_0$, we carry out the linearization of $\gamma$ by numerically estimating the partials matrix $A$. The least squares estimate of $\delta\beta$ is then obtained from Eq. 15 and the following weighting matrix,

$$W = \mathrm{Diag}^{-1}(0.1, 10, 2, 0.01, 0.01, 0.01, 0.25, 0.25, 0.25).$$

This assumes that $\gamma$ is expressed in mm/s, deg/s and m. In order to eliminate imperfections introduced by the linear approximation, the estimation process is iterated until $\delta\beta$ converges to zero. This leads to the estimate of the linear momentum (in body frame):

$$\vec{p} = \begin{pmatrix} -1.5 \\ -1.4 \\ -0.8 \end{pmatrix} \pm \begin{pmatrix} 0.2 \\ 0.5 \\ 0.6 \end{pmatrix} \quad (\text{kg m s}^{-1}). \tag{17}$$

The rotation of $\vec{p}$ to the ORF frame is straightforward. In order to rotate the uncertainties, more precisely the $\mathrm{Cov}(\delta\beta)$ matrix, recall that for any matrix $R$ and vector $x$ we have

$$\mathrm{Cov}(Rx) = R\,\mathrm{Cov}(x)\,R^T. \tag{18}$$

See for example Ref. 6). We thus obtain (in ORF):

$$\vec{p} = \begin{pmatrix} -1.5 \\ -1.6 \\ 0 \end{pmatrix} \pm \begin{pmatrix} 0.2 \\ 0.5 \\ 0.6 \end{pmatrix} \quad (\text{kg m s}^{-1}). \tag{19}$$

The least square fit does not significantly change the estimate of $\vec{r}$. From the above results, it appears that, in the orbital frame, the impacting particle comes neither from below nor above, and hits the back side of the forward solar array. As illustrated in Fig. 8, the incidence angle is about 45 deg with respect to the x-axis of the body frame.

## 5. Particle size estimation

The estimate of the particle linear momentum provides information about its mass. The collision took place near the south pole where, as discussed in Ref. 3), the chance of collision with a man-made debris is the largest. In the following, we use the density of aluminium, 2.8 g/cm$^3$, in order to establish an equivalence between particle mass and size. Size is expressed as the diameter of an equivalent aluminium sphere. The objective of this section is to show that with few additional hypotheses, it is possible to use the result in Eq. 19 to derive a size estimate of the particle. For a more complete analysis, we refer the reader to Ref. 3).

### 5.1. Methodology

The position of the particle at the time of the impact is well determined from the satellite operational orbit constrained by GPS data. The velocity of the particle in an inertial geocentric frame, say the J2000 frame, is constrained by its relative linear momentum, the velocity of the satellite in the geocentric frame and the size of the particle. In consequence, for a given size, the estimate of $\vec{p}$ and the associated uncertainty define a distribution of particle orbital elements in J2000. It is straightforward to determine for each set of elements the associated perigee. Trajectories with perigees smaller than Earth's average radius are clearly unrealistic.

The particle size is estimated by computing, for different sizes, the proportion of realistic cases in the corresponding distributions of possible particle trajectories. Assuming normal distributions for the measurement uncertainties, Eq. 19 provides a multi-variate normal distribution for $\vec{p}$. For the sake of simplicity, we use a very crude sampling of the distribution at the vertices of a box with dimensions given by the uncertainties of the momentum components. For positive or zero values of the uncertainties, this approach would lead to 8 samples. Given that the uncertainties may also have negative values, the sampling includes a total of 27 points. The likelihood of a particle size is obtained by summing the number of realistic samples in the distribution.

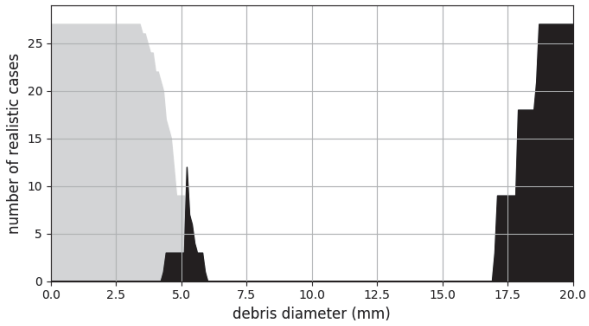


Fig. 9. Number of trajectories with perigee above Earth's mean radius as a function of particle size. Elliptic and hyperbolic trajectories are represented in black and gray respectively.

### 5.2. Results

Fig. 9 provides the evolution of the number of realistic samples as a function of particle size. The evolution is plotted separately for elliptic and hyperbolic trajectories. The presence of man-made debris is to be expected on elliptic trajectories only. Realistic samples appear roughly between 4 mm and 6 mm with a maximum at 5.2 mm. Beyond 17 mm, the number of realistic trajectories grows rapidly to its maximum possible value. The particle is either small and its size well constrained or the particle is relatively large with only a lower limit on its size. The 2 scenarios correspond to, on one hand, a collision with a small particle traveling in an orbital plane approximately perpendicular to the orbital plane of the spacecraft and, on the other hand, a larger particle traveling roughly on the same orbit and in the same direction as the spacecraft. The first scenario is more likely since any particle on the perpendicular orbital plane will encounter the spacecraft many more times than its counterpart. Taking this observation into account, we estimate the particle size at 5 ± 1 mm. This is consistent with the determination in Ref. 3) based on the MASTER-2009 model.

The equivalent mass of the particle is 0.2 ± 0.1 g. With Eq. 19, the relative impact velocity is about 10 km/s. In the second, less likely scenario, the particle mass is at least 7 g and the impact velocity less than 300 m/s.

## 6. Discussion

The uncertainties in the estimated particle momentum depend on the uncertainties of the measurements in Eq. 5, Eq. 6 and Eq. 7. These have been determined by visual inspection of either GPS residuals, the gyro rates or the camera picture. They are thus based, to some extent, on subjective judgment and tend to be rather over-estimated than under-estimated. Recomputing the result in Eq. 19 with uncertainties in $\Delta\vec{\Omega}$ divided by a factor of 2 leads to uncertainties in $p_y$ and $p_z$ also divided by 2. The $p_x$ component is barely affected. Similarly, dividing the uncertainties of $\Delta\vec{V}$ by 2 will divide the uncertainty in $p_x$ by the same factor without affecting $p_y$ and $p_z$. The uncertainty in $\vec{r}$ has no significant effect on any of the components. Unsurprisingly, the $p_x$ component of the linear momentum is mainly determined by

$\Delta\vec{V}$ while the other components are constrained by $\Delta\vec{\Omega}$. It is also interesting to note that for very large uncertainties in $\Delta\vec{V}$, equivalent to the absence of measurement, it is impossible to obtain a meaningful estimation of any of the components of the momentum.

In the past, many anomalies in satellite telemetry have been attributed to collisions with space particles. However finding definite proof of such an event is in general difficult, see for example Ref. 7). The event analyzed in this paper is unique because of the evidence from the on-board camera. Besides the present analysis, the picture allowed to rapidly understand and localize the damage. This leads to the suggestion that on-board cameras should be considered more consistently in future spacecraft designs.

Within the FD system, the spacecraft is operated in a semi-automatic setup. The weekly execution of maneuvers requires the intervention of a FD operator only on Tuesday, Wednesday and Thursday. The system is otherwise running automatically. In particular, it ensures daily orbit determination, based on the latest available GPS data, and the delivery of associated FD routine products. The semi-automatic setup allows to run the operations with a good balance of, on one hand, the workload of the FD team and, on the other hand, the quality of the delivered products. However its semi-automatic character leaves intervals during which a minor anomaly on the satellite may not be immediately detected by the FD system. The collision event occurred on a Tuesday afternoon and went undetected by the FD system until Thursday morning. The event was not detected earlier than Thursday morning due to the exact timing of the automatic and manual operations and, though visible to the eye of an operator, the effects on telemetry were minor and did not trigger any rejection within the automatic system.

The main body of the spacecraft was missed by only 4.6 m in along-track separation, which given the orbital velocity corresponds to less than a millisecond. An impact into the main body followed by a potentially major fragmentation would have triggered a fragment cloud with only extremely limited escape options for any other co-planar satellite (Sentinel-1B in particular). This became already apparent by several conjunctions of the Sentinel-1A tracked fragments with Sentinel-1B and Proba-2. This extra risk will diminish to the background risk level in the course of the next few months. The investigation of the collision event made apparent the need for both Sentinel-1 satellites of a prepared emergency plan in case of a catastrophic disruption of one of the spacecraft.

## 7. Conclusion

We presented a FD analysis of the collision event experienced by Sentinel-1A on August 23$^{rd}$ 2016, at 17:07:37 UTC. The spacecraft was hit on the backside of its forward solar array. Seen from the orbital reference frame, the impacting particle came from a direction of approximately 45 deg with respect to the along track direction. Assuming a man-made aluminium debris, the solar array was impacted by a particle of 5 ± 1 mm in equivalent sphere diameter at a velocity of about 10 km/s.

## Acknowledgments

The first author thanks GMV for the organizational and financial support allocated for attending the ISSFD symposium.

## References

1) R. Torres, P. Snoeij, D. Geudtner, D. Bibby, M. Davidson, E. Attema, P. Potin, B. Rommen, N. Floury, M. Brown, I. Navas Traver, P. Deghaye, B. Duesmann, B. Rosich, N. Miranda, C. Bruno, M. L'Abbate, R. Croci, A. Pietropaolo, M. Huchler, F. Rostan: *GMES Sentinel-1 mission*, Remote Sensing of Environment, Vol. 120, 2012.
2) M. Serrano, I. Shurmer, X, Marc: *Sentinel-1: Operational Approach to the Orbit Control Strategy*, 23rd International Symposium on Space Flight Dynamics, Pasadena, 2012.
3) H. Krag, M. Serrano, V. Braun, P. Kuchynka, M. Catania, J. Siminski, M. Schimmerohn, X. Marc, D. Kuijper, I. Shurmer, A. O'Connoll, M. Otten, Isidro Munoz, J. Morales, M. Wermuth, D. McKissock: *A 1 cm Space Debris Impact onto the Sentinel-1A Solar Array*, Acta Astronautica, Accepted, 2017.
4) M. Oda, Y. Hagiwara, S. Suzuki, T. Nakamura, N. Inaba, H. Sawada, M. Yoshii, N. Goto: *Measurement of Satellite Solar Array Panel Vibrations Caused by Thermal Snap and Gas Jet Thruster Firing*, Recent Advances in Vibrations Analysis, N. Baddour (Ed.), InTech, 2011.
5) P. Kuchynka, W. M. Folkner: *A new approach to determining asteroid masses from planetary range measurements*, Icarus, Vol. 222, Issue 1, 2013.
6) P.J. Bickel, K.A. Doksum: *Appendix A & B*, Mathematical Statistics: Basic Ideas and Selected Topics, vol. I, 2001.
7) *High-Speed Particle Impacts Suspected in Two Spacecraft Anomalies*, Orbital Debris Quarterly News, Vol. 17, Issue 3, 2013.